Nanotechnology and Nano-Interface Controlled Electronic Devices
Editors: M. Iwamoto, K. Kaneto and S. Mashiko

CHAPTER 10

Electrical characterization of organic semiconductor films by in situ field-effect measurements

Kazuhiro Kudo

Department of Electronics and Mechanical Engineering, Faculty of Engineering, Chiba University, 1-33 Yayoi-cho, Inage-ku, Chiba 263-8522, Japan

1. Introduction 157
2. Experimental details of in situ field-effect measurements 158
3. Field-effect characteristics of organic films 160
   3.1. Merocyanine evaporated films 160
   3.2. Phthalocyanine evaporated films 162
   3.3. Hole transporting materials for EL devices 168
   3.4. Perylene evaporated films 173
4. Conclusions 178
References 179

1. Introduction

Organic semiconductors have recently received increasing interest because of their potential applications in low-cost and large-area devices such as organic light emitting diodes (LEDs), organic field-effect transistors (FETs), and optoelectronic integrated circuits (OEIC). High carrier mobilities comparable to amorphous silicon have been obtained for several organic transistor materials. In particular, field-effect mobilities in the range from 1 to 5 $cm^2/V\,s$ and on/off current ratios larger than 10^8 were reported in single crystal organic FETs [1–3]. Although many kinds of p-type organic semiconductors have been reported, there are few examples of n-type behavior. For practical device applications, both p-type and n-type semiconducting materials with high stability against air are highly desirable. From these points of view, it is important to investigate the intrinsic electrical properties of organic semiconductor films before and after exposing in atmospheric gasses, especially oxygen gas. In situ field-effect measurement is a promising method for the evaluation of conduction type (p or

n), carrier mobility (μ), electrical conductivity (σ), and carrier concentration (N) of evaporated films [4,5].

Phthalocyanine (Pc) and merocyanine (MC) derivatives have potential for application to organic electronic devices, such as gas sensors [6,7] and optoelectronic devices [8,9] because of their p-type semiconducting properties and absorption bands which extend from the ultraviolet to the infrared region. In particular, the coordinated metals in Pc are important factors for the photoelectrical properties. It is necessary to investigate the relationship between their chemical structure and intrinsic electrical properties, especially without the influence of atmospheric gasses and impurities. The in situ field-effect measurement [4,5] is a promising method to evaluate the electrical parameters of organic thin films.

In the present work, we have carried out the in situ field-effect measurement of several kinds of organic semiconductors expected for optoelectronic devices, and estimated the intrinsic electrical parameters, such as carrier mobility (μ), carrier concentration (N) and electrical conductivity (σ), and excluded the influence of atmospheric gasses and impurities with in situ field-effect measurements. The organic films were fabricated by a standard vacuum evaporation technique and the FET characteristics were investigated before and after breaking the vacuum by oxygen gas, and the thermal treatment. Furthermore, the conduction process is discussed with the experimental results.

2. Experimental details of in situ field-effect measurements

A schematic of an in situ field-effect measurement system and the sample structure are shown in Figs. 1 and 2. The highly doped Si substrate which works as a gate electrode was covered with thermally grown SiO_2 with a thickness of approximately 200 nm. The interdigital source and drain electrodes were formed on the substrate using standard vacuum evaporation and photolithographic techniques. The metal materials of the source and drain electrodes were chosen to make an ohmic contact to the organic

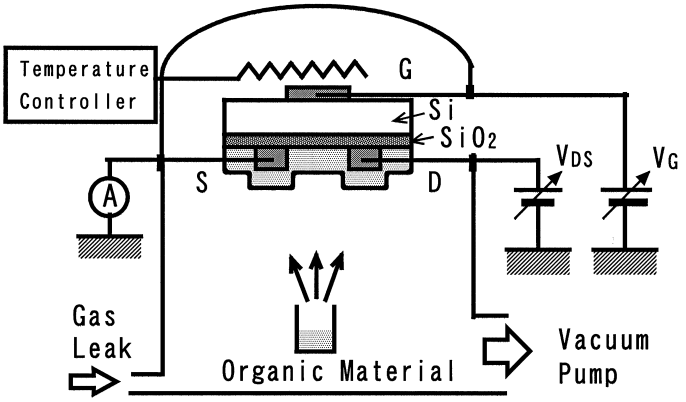

Fig. 1: Schematic of the in situ field-effect measurement.

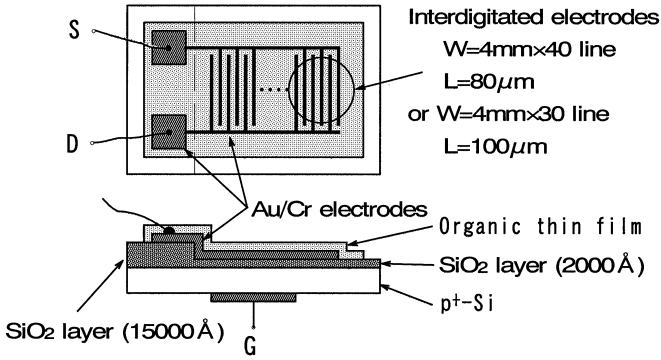

Fig. 2: Schematic of the sample structure of the in situ field-effect measurement.

materials, i.e., Au for p-type organic films and In for n-type films. The channel length and width were 0.1 and 56 mm, respectively. Substrates were thoroughly cleaned with organic solvent in an ultrasonic bath and prebaked at 373 K over 30 min in the vacuum chamber. Subsequently, organic semiconductor materials were evaporated as the active component of the FET. During the evaporation, substrate temperature, T_{sub}, was controlled depending on the organic materials from room temperature to 100°C (373 K). Typical thickness of the organic films was approximately 200 nm. Field-effect measurements were performed immediately after the evaporation of organic thin film, after the exposure to oxygen gas for 5 h, and after the thermal annealing of the sample at 373 K for 1 h in vacuum (10^{-5} Torr). All of the electrical measurements were carried out in the dark.

The characteristics of the source–drain current (I_{DS}) vs source–drain voltage (V_{DS}) with applying gate voltage (V_G) were measured. I_{DS} in the linear region for a standard TFT is given by [10]

$$I_{DS} = -(W/L)C_{OX}[(V_G - V_{th})V_{DS} - (1/2)V_{DS}^2], \tag{1}$$

where W is the channel width, L is the channel length, μ is the carrier mobility, C_{OX} is the capacitance of the SiO_2 layer, and V_{th} is the threshold voltage. When I_{DS} does not increase at higher V_{DS} (saturation region), I_{DS} is expressed by [10]

$$I_{DS} = -(W/2L)\mu C_{OX}(V_G - V_{th})^2. \tag{2}$$

According to Eq. 2, μ can be obtained by plotting $(V_{DS})^{1/2}$ against V_G. The electrical conductivity (σ) was obtained from the slope of the I_{DS}–V_{DS} plot at $V_G = 0$. σ is also expressed by

$$\sigma = qN\mu, \tag{3}$$

where q is the elementary electric charge and N is the carrier concentration. N was obtained from Eq. 3.

3. Field-effect characteristics of organic films

3.1. Merocyanine evaporated films

Merocyanine (MC) derivatives are reported as p-type semiconducting materials and their photovoltaic effects were shown in Schottky diode or pn junction cells [6–8]. In this study, we have estimated their parameters such as field-effect mobility, carrier concentration, and electrical conductivity by field-effect measurements and discussed the transport mechanism of MC film from the temperature dependence of the FET characteristics.

Fig. 3 shows the molecular structures of MC derivatives examined here. Typical characteristics of I_{DS} vs V_{DS} measured for MC(a) FET are shown in Fig. 4. I_{DS} increases with negative V_G and MC TFT operates in an enhancement mode. This result indicates that negative gate voltages form a hole accumulation layer and MC films show p-type semiconducting properties without influences of impurities and atmospheric gasses. From this procedure, the following electrical parameters of MC(a) film were estimated: the field-effect mobility was 1.4×10^{-6} cm^2/V s, the electrical conductivity was 2.6×10^{-10} S/cm, and the carrier concentration was 1.3×10^{15} cm^{-3}. The estimated value of μ depends on the thickness of the dye films. Fig. 5 shows μ variation as a function of film thickness of MC(a), MC(b), and MC(c). As the film thickness increases, μ increases and saturates at about 200 nm. These phenomena are mainly due to the effects of interface traps between SiO_2 and organic film, and the carrier conduction of the discontinuous parts in thin films. Both effects appear strongly in thinner films and tend to be inconspicuous in thicker films. From this result, we have chosen as standard thickness of the organic films 200 nm.

Table 1 shows the field-effect mobilities at the gate and drain bias voltages of 20 V,

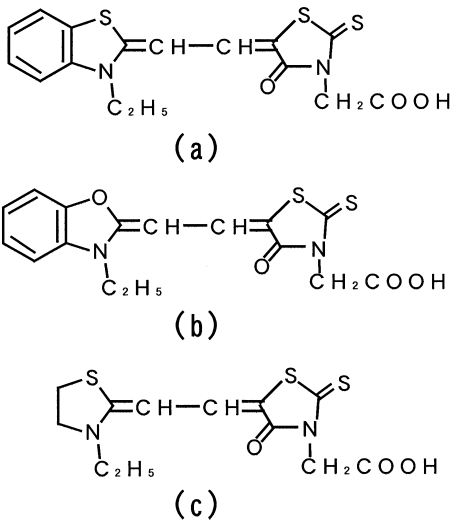

Fig. 3: Molecular structures of MC derivatives examined here.

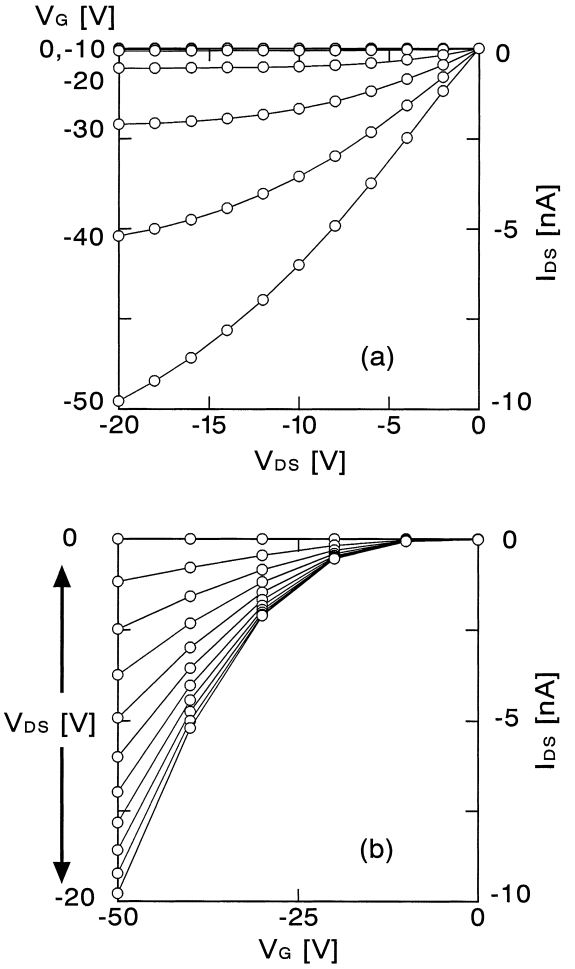

Fig. 4: Typical characteristics of I_{DS} vs V_{DS} measured for MC(a) FET.

Table 1

Field-effect mobility and photoelectric quantum efficiency of merocyanine films

Dye	Field-effect mobility ($cm^2/V\,s$)	Photoelectric quantum efficiency (%)
(a)	1.5×10^{-5}	1.0
(b)	5.0×10^{-6}	0.3
(c)	1.0×10^{-7}	0.1

and the photoelectric quantum efficiencies in the Schottky type cells using MC dyes (Fig. 3(a), (b) and (c)). The quantum efficiencies were roughly estimated using the illuminated monochromatic photon density and electrons produced as a short-circuit

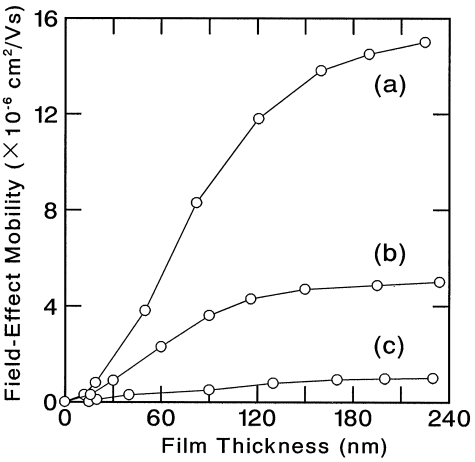

Fig. 5: Carrier mobility variation as a function of the film thickness of MC(a), MC(b), and MC(c).

photocurrent [8]. It should be noted that the photoelectric quantum efficiencies are closely related to the field-effect mobilities.

The temperature dependence of electrical parameters obtained by in situ field-effect measurement is shown in Fig. 6. From these Arrhenius plots, the activation energies of conductivity and field-effect mobility in MC film were estimated to be 0.44 eV, and the activation energy of carrier concentration was very low (0.04 eV). These results indicate that the generation of thermally activated carriers from the shallow acceptor level is very low and there are few carriers directly excited from the band to band or HOMO (highest occupied molecular orbital) to LUMO (lowest unoccupied molecular orbital) level in this temperature region. Furthermore, the field-effect mobility is thermally activated, and hopping conduction, which is often employed in molecular films [11,12], is adequate as a main transport mechanism of MC film. Most of the hole carriers are trapped at the hopping sites of the potential well of the valence band or HOMO level. The carrier concentration estimated by the field-effect measurements in the previous section represents the number of hopping carriers.

3.2. Phthalocyanine evaporated films

Phthalocyanine (Pc) films have been expected as gas sensors [6,7] and the coordinated metals in Pc are important factors for their electrical properties. It is necessary to investigate the relationship between their chemical structure and intrinsic electrical properties, especially without the influence of atmospheric gasses and impurities. As Pc derivatives, copper-phthalocyanine (CuPc), lead-phthalocyanine (PbPc), metal-free phthalocyanine (H_2Pc), and fluoro-phthalocyanine (F_{16}CuPc) were examined here, and n-type behavior of F_{16}CuPc was reported [13,14]. Fig. 7 shows the molecular structures of the Pc derivatives and these materials were purified by the sublimation method.

Typical FET characteristics (I_{DS} vs V_{DS} as a function of V_G) of a CuPc sample after the deposition at T_{sub} of 373 K are shown in Fig. 8(a). I_{DS} increases with negative

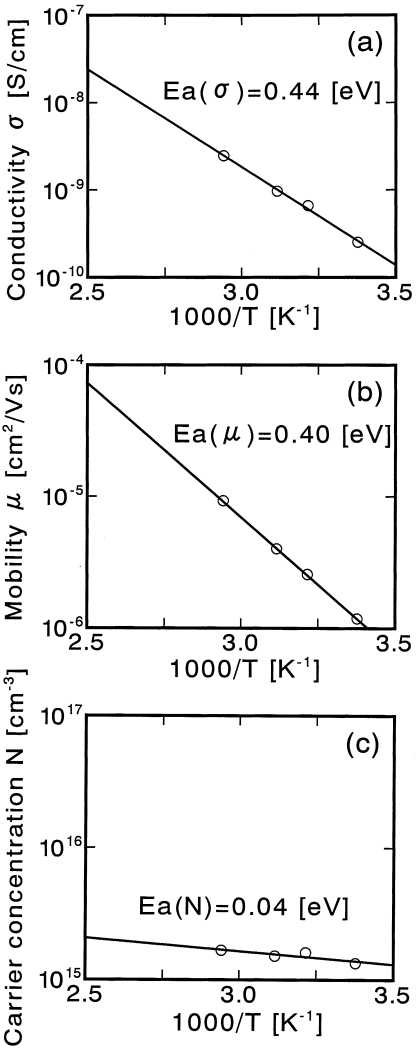

Fig. 6: Temperature dependence of electrical parameters obtained by in situ field-effect measurement.

V_G and the CuPc FET operates in an enhancement mode. This result indicates that negative gate voltages enlarge the conduction channel due to the formation of a hole accumulation layer, thus, CuPc films show p-type semiconducting properties. We have also investigated the effect of oxygen gas and annealing on the electrical properties of the films. Fig. 8(b) and (c) shows FET characteristics of the CuPc sample after the oxygen gas exposure and after the thermal treatment in vacuum, respectively. Although the I_{DS} increases after the oxygen gas exposure, the I_{DS} decreases by the thermal treatment at 373 K in vacuum for 1 h. It was also confirmed that H_2Pc and PbPc showed p-type semiconducting properties in the absence of atmospheric gasses. However, the

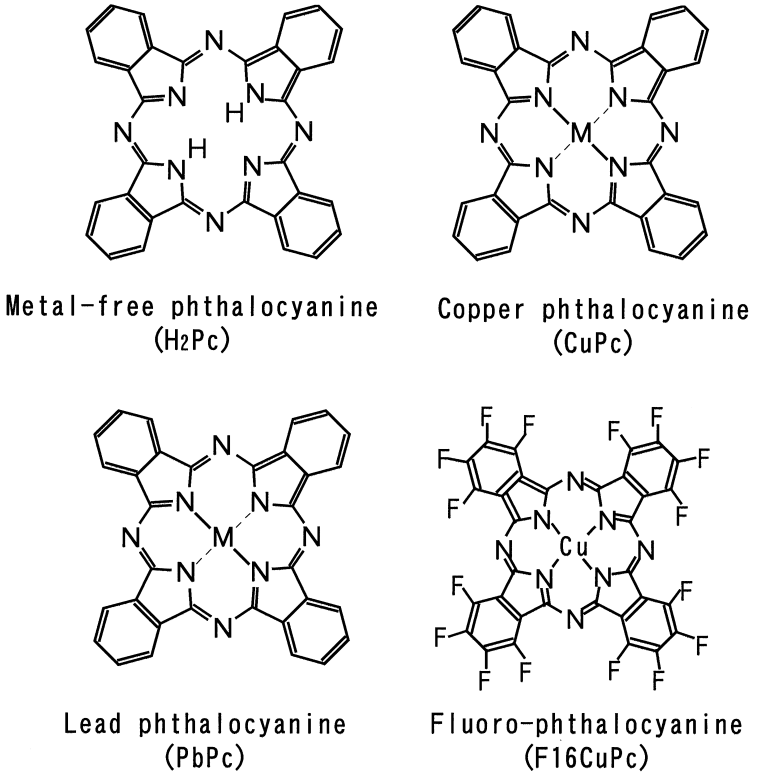

Fig. 7: Molecular structures of Pc derivatives.

effect of oxygen gas on the FET characteristics depends on the molecular species. Comparing FET characteristics of these p-type materials, the effect of oxygen on PbPc film is significant but that on H_2Pc films is small.

On the other hand, typical FET characteristics of $F_{16}CuPc$ films are shown in Fig. 9. Electrical properties of $F_{16}CuPc$ films are rather stable against the oxygen gas exposure. The experimental results in Table 2 and Fig. 9 indicate that the influence of oxygen gas exposure is small and the fluorine atoms in $F_{16}CuPc$ molecules seem to prevent oxygen adsorption.

The carrier mobility, μ, conductivity, σ, and carrier concentration, N obtained by the in situ field-effect measurements are shown in Table 2. Fig. 10 shows the variations of N and μ of as-grown sample, after oxygen gas exposure and after annealing in vacuum.

It is noteworthy that the most significant change in N occurs upon the exposure to oxygen gas. Particularly in PbPc films, N increased when the sample was exposed to oxygen gas and decreased when the sample was annealed in vacuum. The effect of oxygen on N is marked in PbPc films compared with those in H_2Pc and $F_{16}CuPc$ films. The effect of oxygen on CuPc film is between those of the PbPc and H_2Pc films. Thus, oxygen gas acts as an acceptor impurity and increases the net charge carriers. It is considered that electrons transfer from phthalocyanine molecules to oxygen molecules

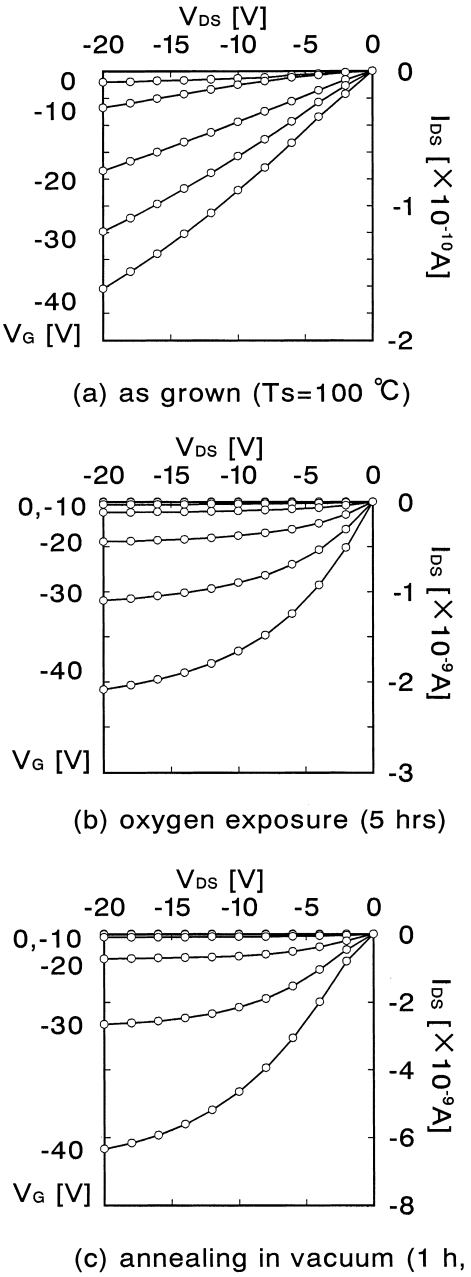

Fig. 8: Typical FET characteristics of a CuPc sample, (a) as-grown at T_{sub} of 373 K, (b) oxygen exposure (5 h), (c) annealing at 373 K in vacuum (1 h).

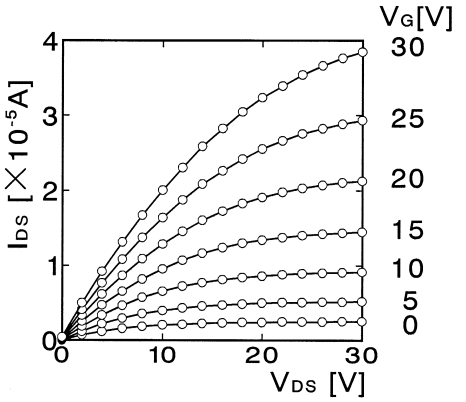

(a) as grown

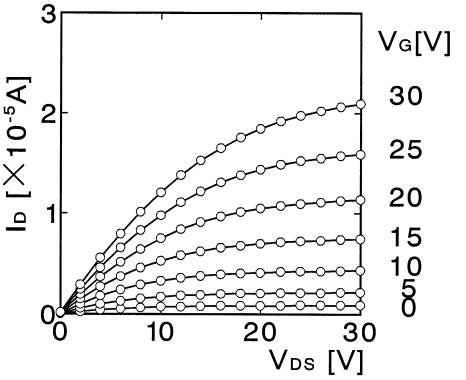

(b) oxygen exposure (5 hrs)

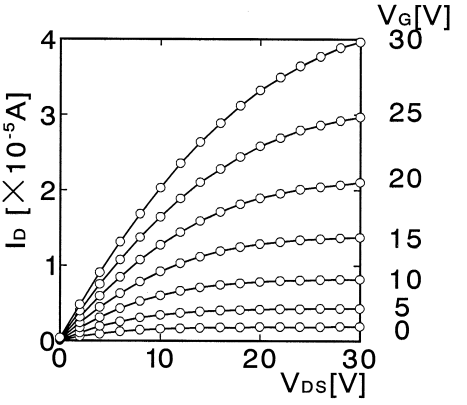

(c) annealing in vacuum (1 h)

Fig. 9: Typical FET characteristics of F_{16}CuPc films, (a) as-grown, (b) oxygen exposure (5 h), (c) annealing at 373 K in vacuum (1 h).

Table 2
Electrical parameters of phthalocyanine derivatives obtained by in situ field-effect measurements

Material	T_{sub} (K)	As-grown	O_2 gas exposure	Annealing in vacuum
Hole mobility (cm^2/Vs)				
PbPc	373	3.8×10^{-6}	5.7×10^{-5}	3.2×10^{-5}
CuPc	373	2.4×10^{-6}	1.2×10^{-5}	1.1×10^{-5}
H_2Pc	373	2.0×10^{-6}	2.1×10^{-6}	3.6×10^{-6}
$F_{16}CuPc$	373	1.6×10^{-3}	1.0×10^{-3}	1.8×10^{-3}
Conductivity (S/cm)				
PbPc	373	1.3×10^{-9}	7.7×10^{-7}	6.6×10^{-8}
CuPc	373	2.1×10^{-10}	4.6×10^{-10}	1.3×10^{-9}
H_2Pc	373	1.1×10^{-10}	1.4×10^{-10}	7.5×10^{-11}
$F_{16}CuPc$	373	5.6×10^{-5}	2.1×10^{-5}	4.4×10^{-5}
Carrier concentration (cm^{-3})				
PbPc	373	2.1×10^{15}	8.4×10^{16}	1.3×10^{16}
CuPc	373	5.4×10^{14}	2.4×10^{15}	8.2×10^{14}
H_2Pc	373	3.4×10^{14}	4.1×10^{14}	1.3×10^{14}
$F_{16}CuPc$	373	2.2×10^{17}	1.2×10^{17}	1.5×10^{17}

and oxygen molecules are directly related to the composition of the central metal of phthalocyanine molecules. This result is closely related to reports that the interaction between H_2Pc and oxygen is weak [15] or that the adsorption site of H_2Pc is different from that of metal phthalocyanines [16].

$F_{16}CuPc$ has the largest mobility and H_2Pc the smallest, indicating that the carrier mobility is dependent on the coordinated metal and fluorine atoms. These seem to be intrinsic properties of the materials measured, since the effect of oxygen was excluded during measurements. It should be noted that the deposition at high temperature gave high μ for all Pc films.

Evaluation of the thermal activation energy (E_a) is important to discussion of the carrier transport mechanism in organic semiconducting films. In particular, the temperature dependence of σ, μ, and N is necessary, because E_a estimated by σ contains both μ and N, as expressed in Eq. 3. Fig. 11 shows $E_a(\sigma)$, $E_a(\mu)$, and $E_a(N)$ estimated by Arrhenius plots between 295 and 380 K for CuPc film. Plots of $\log\sigma$, $\log\mu$, $\log N$ against $1/T$ follow a straight line. The carrier mobility of CuPc film has an activation energy of about 0.26 eV. $E_a(\mu)$ obtained by the field-effect measurement can be interpreted in terms of a barrier which prevents the carrier transport at the interface between the micrograins or between the organic film and the electrodes. The effect of oxygen on $E_a(\sigma)$ and $E_a(N)$ depends on the chemical structure of the Pc molecules. Although E_a of $F_{16}CuPc$ and H_2Pc remain almost the same values, those of PbPc and CuPc change to lower values after the oxygen exposure. In particular, $E_a(\sigma)$ of PbPc film varied from 0.53 to 0.23 eV by introducing oxygen gas. After thermal treatment in vacuum, $E_a(\sigma)$ recovers to almost the same value of 0.54 eV. These results indicate that oxygen molecules interact with the PbPc molecules and a shallow acceptor level is formed near the valence band edge or HOMO (highest occupied molecular orbital) level

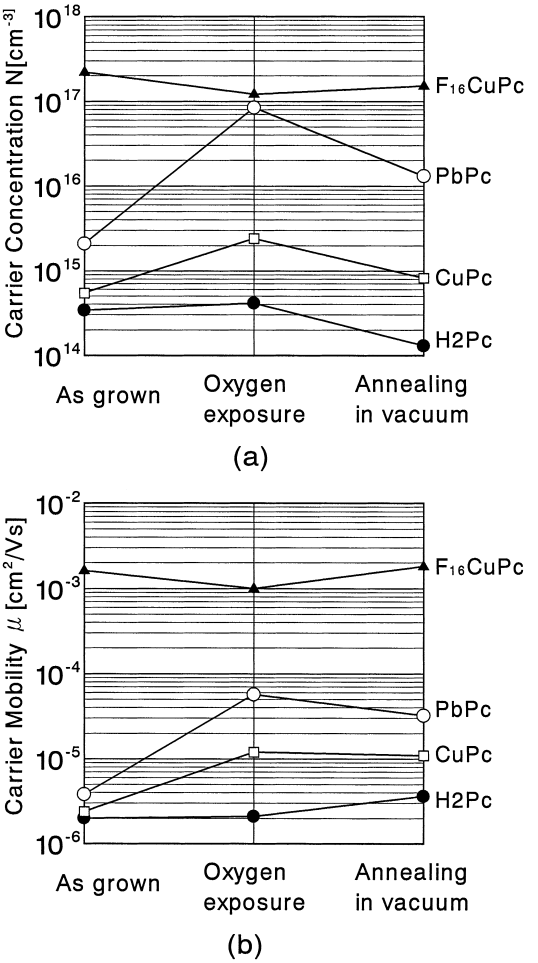

Fig. 10: The variations of N and μ of as-grown sample, after oxygen gas exposure and after annealing in vacuum.

of the PbPc. Thus, oxygen gas acts as an acceptor impurity and increases the net charge carriers.

3.3. Hole transporting materials for EL devices

Organic electroluminescent (EL) devices have already been put to practical use for display panels. However, basic electrical parameters of organic materials used in EL devices have been hardly reported. Thin-film transistors (TFTs) using hole transporting materials of organic EL devices were fabricated and the electrical parameters were estimated by in situ field-effect measurements. Fig. 12 shows molecular structures of TPD (N,N'-diphenyl-N,N'-di(3-methylphenyl)-1,1′-biphenyl-4,4′-

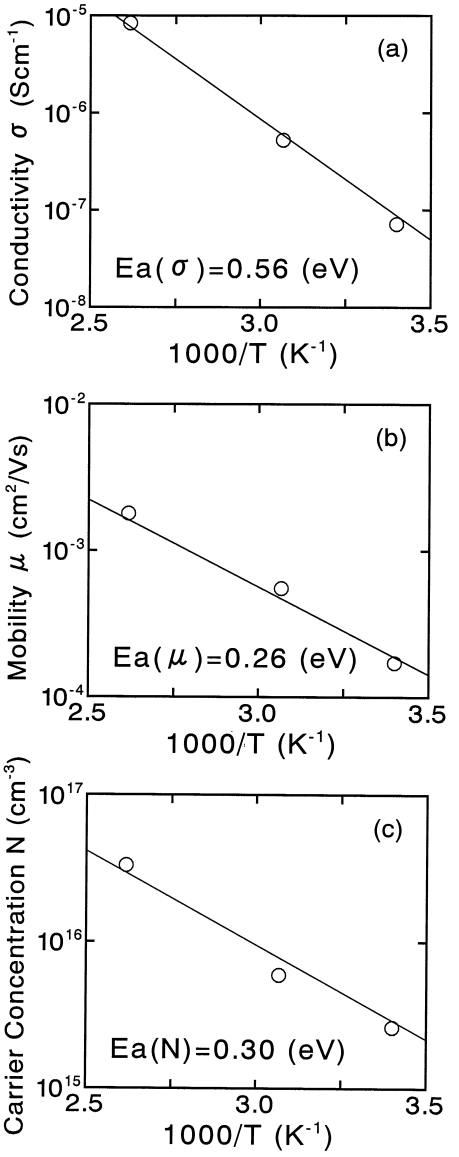

Fig. 11: Arrhenius plots of σ, μ, and N between 295 and 380 K for CuPc film.

diamine), a-NPD (N,N'-diphenyl-N,N'-di(1-napthyl)-1,1′-biphenyl-4,4′-diamine), and m-MTDATA (4,4′,4″-tris-(3-methylphenyl-phenylamino)triphenylamine). The growth temperatures (T_{sub}) of these materials were selected below the glass transition temperature (T_g). The glass transition temperatures of TPD, a-NPD, and m-MTDATA are 63, 96, and 75°C, respectively.

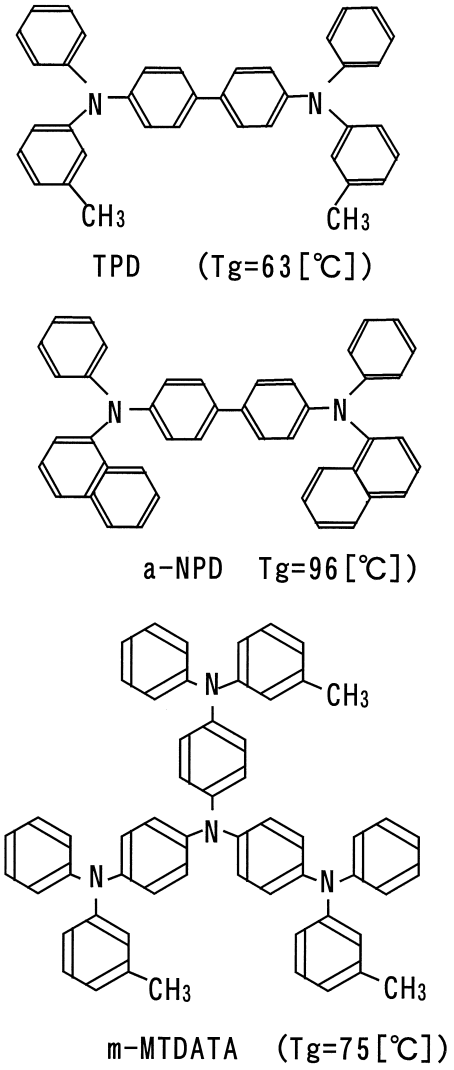

Fig. 12: Molecular structures of TPD, a-NPD, and m-MTDATA.

Typical FET characteristics of TPD, a-NPD and m-MTDATA just after deposition are shown in Figs. 13(a), (b), and (c), respectively. For all the materials, I_{DS} increases with increasing negative V_G. These results indicate that a hole accumulation layer is formed by negative gate voltages and evaporation films of hole transport materials have p-type semiconducting properties. From these results, the estimated field-effect carrier mobilities of TPD, a-NPD, and m-MTDATA were 1.6×10^{-6}, 9.3×10^{-8}, and 6.3×10^{-7} $cm^2/V\,s$, respectively (Table 3). These values of μ are smaller than those obtained by the time-of-flight method [17]. The difference in the μ values using the FET

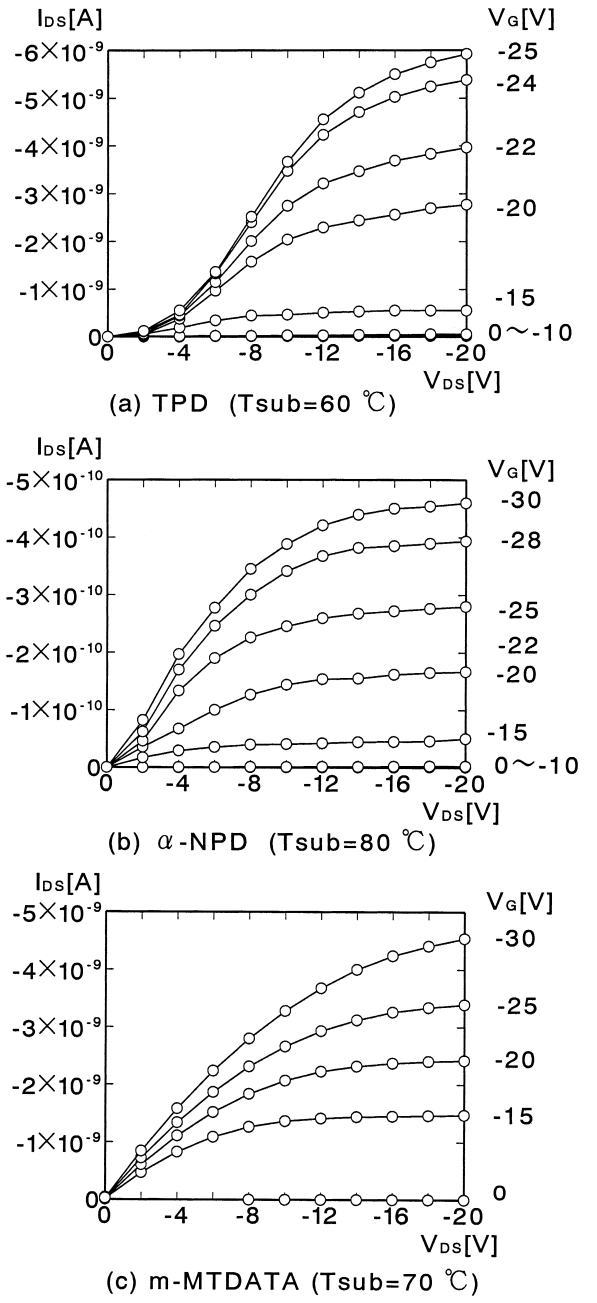

Fig. 13: Typical FET characteristics of TPD, a-NPD and m-MTDATA just after deposition.

Table 3
Electrical parameters of hole transporting materials obtained by in situ field-effect measurements

Material	T_{sub} (K)	As-grown	O_2 gas exposure	Annealing in vacuum
Hole mobility (cm^2/Vs)				
TPD	333	1.6×10^{-6}	1.3×10^{-6}	2.3×10^{-6}
α-NPD	353	9.3×10^{-8}	2.3×10^{-7}	3.2×10^{-7}
m-MTDATA	343	6.3×10^{-7}	6.0×10^{-7}	6.2×10^{-7}
Conductivity (S/cm)				
TPD	333	1.3×10^{-11}	8.1×10^{-12}	7.6×10^{-12}
α-NPD	353	1.1×10^{-12}	9.4×10^{-13}	6.5×10^{-12}
m-MTDATA	343	1.7×10^{-10}	2.4×10^{-10}	1.3×10^{-10}
Carrier concentration (cm^{-3})				
TPD	333	2.2×10^{13}	2.6×10^{13}	1.1×10^{13}
α-NPD	353	7.6×10^{13}	3.6×10^{13}	1.3×10^{14}
m-MTDATA	343	1.7×10^{15}	2.5×10^{15}	1.3×10^{15}

and time-of-flight method is probably due to the difference in the electric field, current direction though the organic films, etc.

Fig. 14 shows the variations of N and μ of as-grown sample, after oxygen gas exposure and after annealing in vacuum. As shown in Fig. 14(a) and (b), these hole transporting materials show stable against the oxygen exposure. Fig. 15 shows the electrical properties of TPD, a-NPD, and m-MTDATA films as a function of substrate temperature (T_{sub}) during the deposition. The conductivity of m-MTDATA is higher than that of the other materials. The conductivities of a-NPD and m-MTDATA have weak dependence on T_{sub} below T_g. However, the conductivity of TPD has a peak at around 55°C. The conductivities of all the materials show a drastic change at T_{sub} over T_g. The carrier mobilities of these materials show clearer T_{sub} dependence. The carrier mobility of a-NPD and m-MTDATA changes to a low value under T_g, the carrier mobility of m-MTDATA is one order larger than that of a-NPD. On the other hand, the carrier mobility of TPD has a sharp peak at T_{sub} around 55°C.

Similar phenomena were observed by the thermal treatment in air after the film deposition. The electrical properties of all the materials show a drastic change after the thermal treatment over T_g. Fig. 16 shows AFM (atomic force microscope) images of TPD films after thermal treatment below and above T_g. Though the surface of the TPD film after the thermal treatment at 50°C ($< T_g$) was completely flat (Fig. 16(a)), the morphology of the film after the thermal treatment at 70°C ($> T_g$) changed to that of an island-like film (Fig. 16(b)). The steepness of the change in electrical properties at a higher temperature is mainly due to the discontinuity of the conductive channel caused by the formation of island-like grains after the thermal treatment (Fig. 17). These results indicate that the degradation of organic EL devices at higher temperatures is closely related to the formation of island-like grains in hole transport layers at higher temperature over T_g.

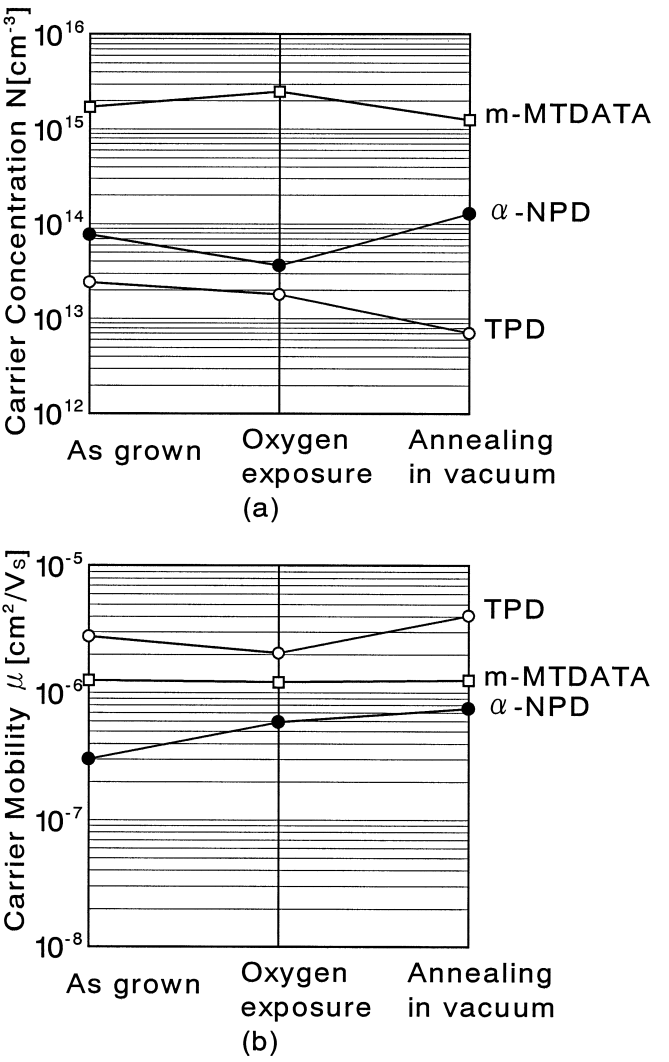

Fig. 14: The variations of N and μ of as-grown sample, after oxygen gas exposure and after annealing in vacuum.

3.4. Perylene evaporated films

Three kinds of perylene derivatives (PTCDI, PTCDA, BPPC) were used and n-type characteristics were reported [18–20]. The chemical structures are shown in Fig.18. These materials purified by sublimation under an argon flow.

Fig. 19 shows typical FET characteristics of PTCDI films. The channel conduction of all perylene derivatives increases with positive V_G and the FETs operate in an enhancement mode. From the results of field-effect measurements, as deposited films of

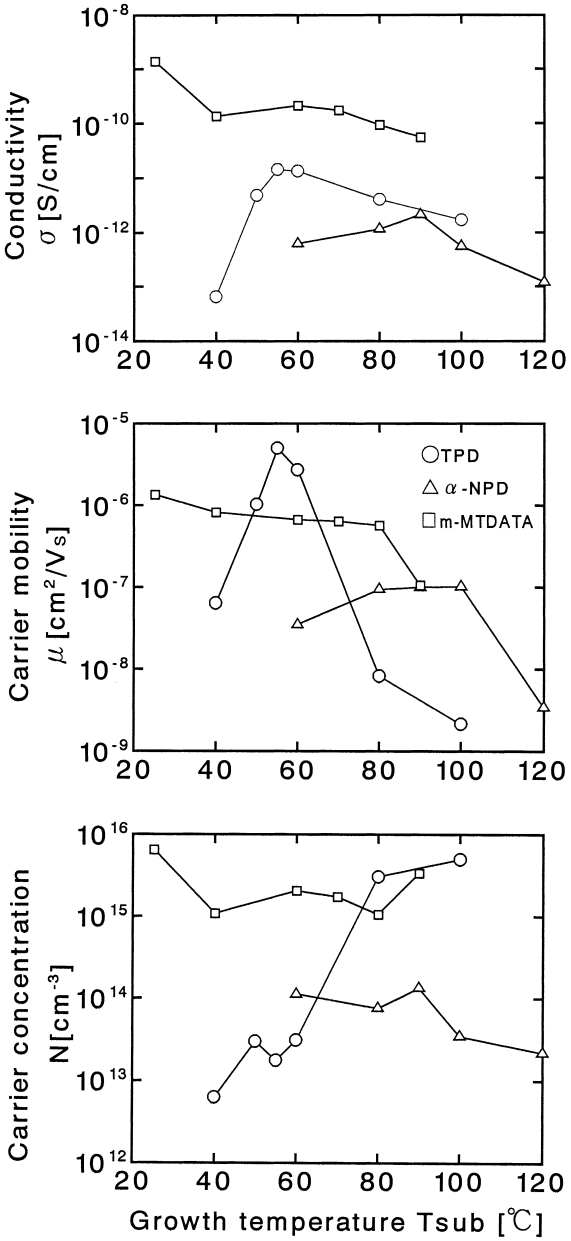

Fig. 15: Electrical properties of TPD, a-NPD, and m-MTDATA films as a function of substrate temperature (T_{sub}) during the deposition.

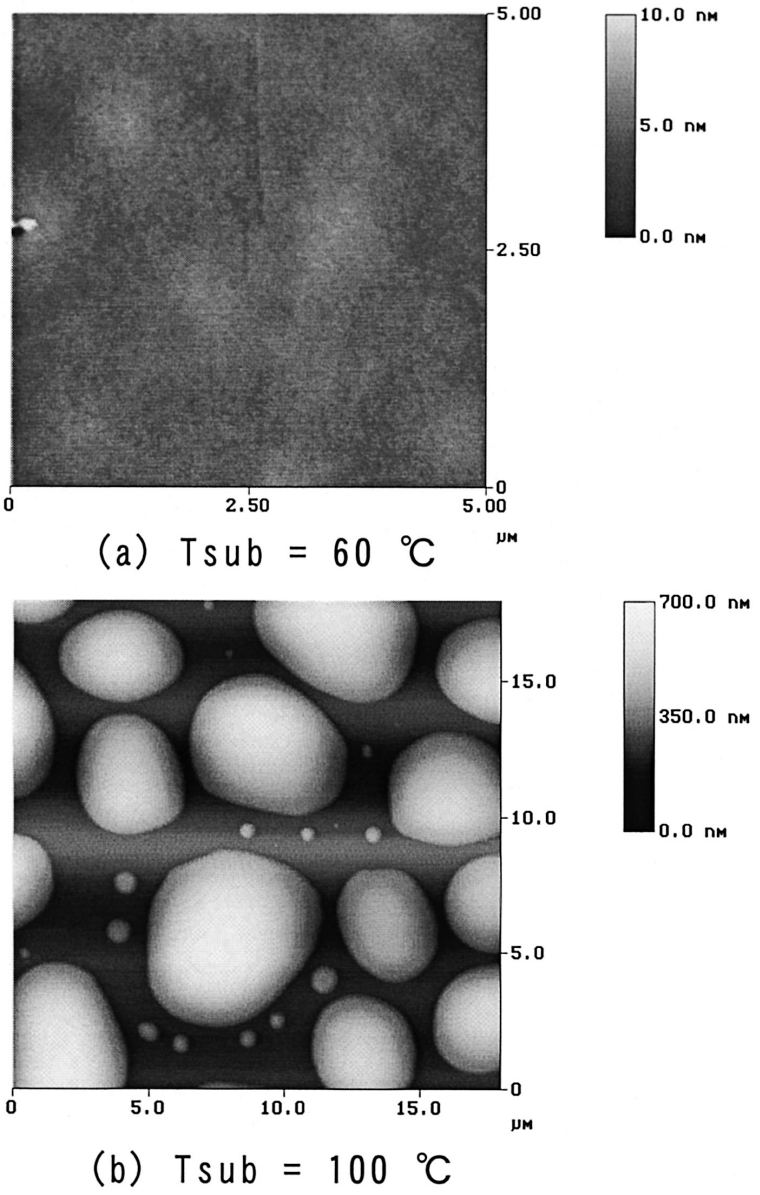

Fig. 16: AFM (atomic force microscope) images of TPD films after thermal treatment below and above T_g.

PTCDI, PTCDA, and BPPC showed n-type semiconducting properties in the absence of atmospheric gasses. The introducing of oxygen gas to the n-type films works to decrease the conductivity and the degree of change depends on the molecular species. FET characteristics of PTCDI film obtained just after the deposition were completely

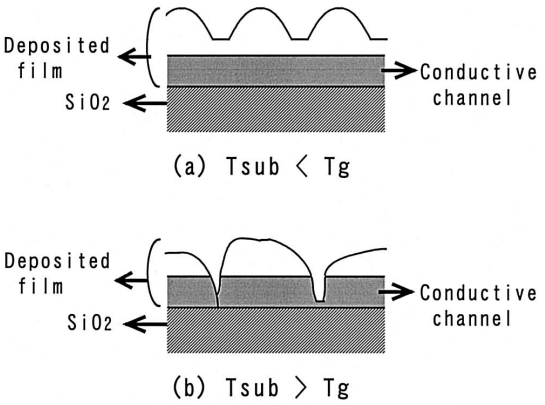

Fig. 17: Change of conduction channel due to island-like grain formation.

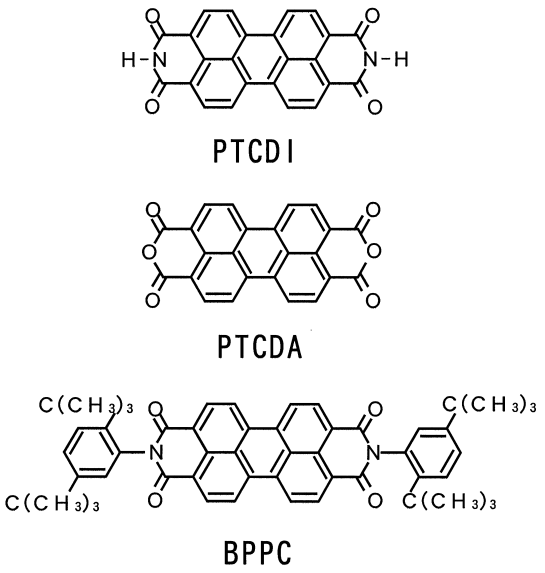

Fig. 18: Molecular structures of perylene derivatives (PTCDI, PTCDA, BPPC).

ruined by the oxygen gas exposure (Fig. 19(b)) and did not recover to the same values as those of as-grown samples.

The hole mobility, μ, conductivity, σ, and carrier concentration, N, obtained by the in situ field-effect measurements are shown in Table 4. The effect of oxygen gas exposure on perylene films is in a marked contrast to that of p-type materials. The variations of N and μ in perylene films are shown in Fig. 20, for as-grown sample, after oxygen gas exposure and after annealing in vacuum. In some cases, oxygen gas acts as an acceptor impurity and produces good results for p-type materials, but oxygen

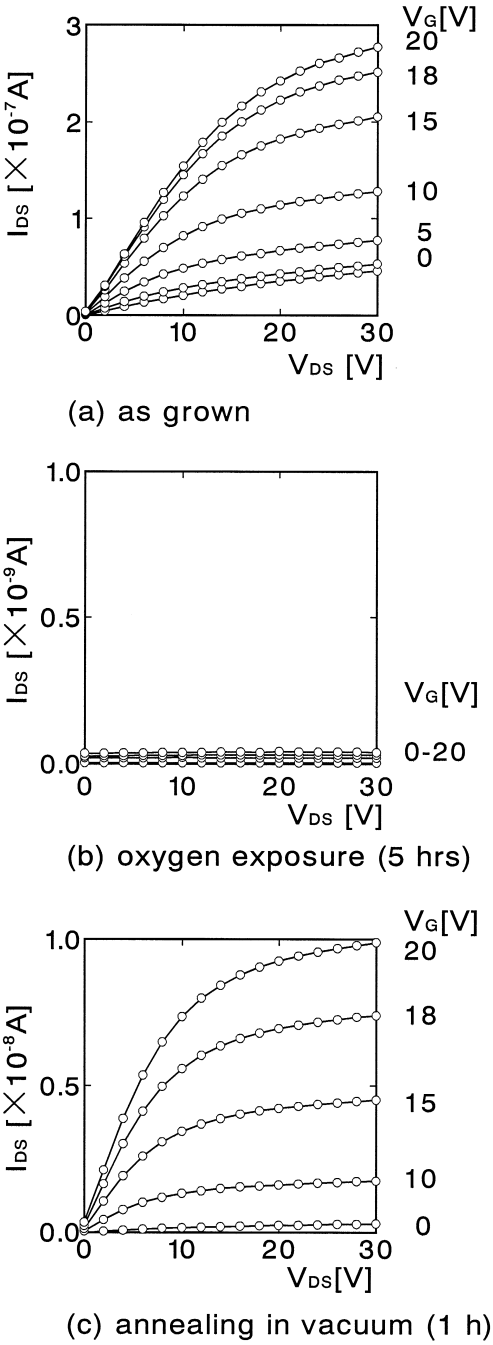

Fig. 19: Typical FET characteristics of PTCDI films.

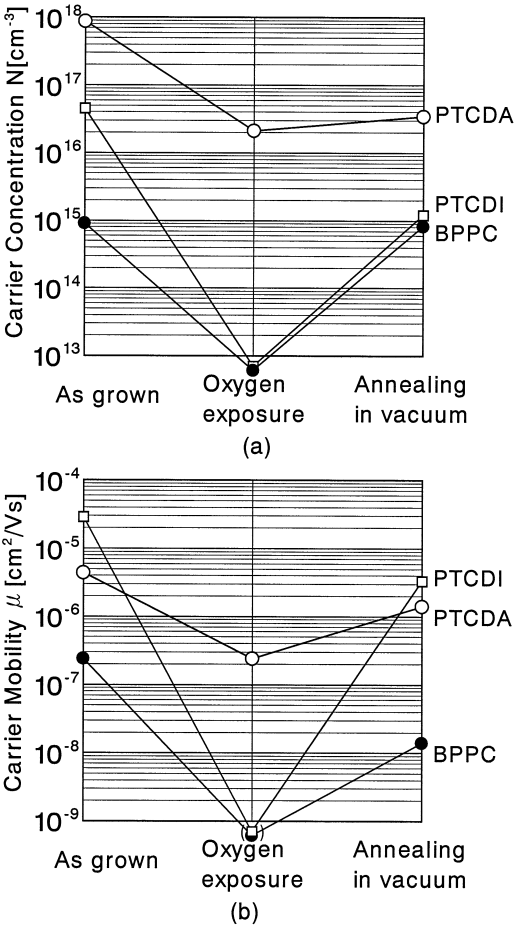

Fig. 20: The variations of N and μ in perylene films.

gas exposure causes serious problems for n-type materials. These phenomena can be explained as follows: oxygen gas acts as an acceptor impurity and carrier compensation occurs in n-type films. The variation of the electrical properties, however, depended on the molecular structure and the growth condition of the films.

4. Conclusions

The basic electric parameters of several kinds of organic thin films were evaluated by in situ field-effect measurement. The effects of thermal treatment and introducing oxygen gas on the electrical properties were also investigated. A marked change in the electrical parameters corresponding to the adsorption and desorption of oxygen molecules was observed and the variation of the electrical properties strongly depended

Table 4
Electrical parameters of perylene derivatives obtained by in situ field-effect measurements

Material	T_{sub} (K)	As-grown	O_2 gas exposure	Annealing in vacuum
Electron mobility (cm^2/Vs)				
PTCDI	373	2.9×10^{-5}	$< 10^{-7}$	3.3×10^{-6}
PTCDA	373	4.4×10^{-6}	2.4×10^{-7}	1.4×10^{-6}
BPPC	373	2.4×10^{-7}	$< 10^{-7}$	1.1×10^{-8}
Conductivity (S/cm)				
PTCDI	373	2.1×10^{-7}	$< 10^{-12}$	6.6×10^{-10}
PTCDA	373	6.1×10^{-7}	8.2×10^{-10}	7.4×10^{-9}
BPPC	373	3.5×10^{-11}	$< 10^{-12}$	1.4×10^{-12}
Carrier concentration (cm^{-3})				
PTCDI	373	4.5×10^{16}	$< 10^{14}$	1.2×10^{15}
PTCDA	373	8.7×10^{17}	2.1×10^{16}	3.4×10^{16}
BPPC	373	9.0×10^{14}	$< 10^{14}$	8.2×10^{14}

on the molecular structure and the growth conditions of the films. These results demonstrate that the influence of atmospheric gases is significant for organic device applications and the in situ field-effect measurement is a powerful method to investigate the fundamental properties of organic materials.

References

1. C.D. Dimitrakopoulos and P.R.L. Malenfant, Adv. Mater. **14**, 99 (2002).
2. H. Klauk, D.J. Grundlach, J.A. Nichols, C.D. Sheraw, M. Bonse, and T.N. Jackson, Solid State Tech. **43**, 63 (2000).
3. C.R. Kagan, D.B. Mitzi, and C.D. Dimitrakopoulos, Science **286**, 945 (1999).
4. K. Kudo, M. Yamashina, and T. Moriizumi, Jpn. J. Appl. Phys. **23**, 130 (1984).
5. K. Kudo, T. Sumimoto, K. Hiraga, S. Kuniyoshi, and K. Tanaka, Jpn. J. Appl. Phys. **36**, 6994 (1997).
6. C. Hamann, A. Mrwa, M. Muller, W. Gopel, and M. Rager, Sens. Actuat. B **4**, 73 (1991).
7. A. Wilson, J.D. Wright, and A.V. Chadwick, Sens. Actuat. B **4**, 499 (1991).
8. A.K. Ghosh, D.L. Morel, T. Feng, R.F. Shaw, and C.A. Rowe Jr., J. Appl. Phys. **45**, 230 (1974).
9. K. Kudo, T. Shinohara, T. Moriizumi, K. Iriyama, and M. Sugi, Jpn. J. Appl. Phys., Suppl. **20-2**, 135 (1981).
10. S.M. Sze, *Physics of Semiconductor Devices* (Wiley, New York, 1969) p. 425.
11. K. Kaneto, K. Yamanaka, K. Rikitake, T. Akiyama, and W. Takashima, Jpn. J. Appl. Phys. **35**, 1802 (1996).
12. H. Bassler, G. Schonherr, M. Abkowitz, and D.M. Pai, Phys. Rev. B **26**, 3105 (1982).
13. Z. Bao, A.J. Lovinger, and A.Dodabalapur, Adv. Mater. **9**, 42 (1997).
14. Z. Bao, A.J. Lovinger, and J. Brown, J. Am. Chem. Soc. **120**, 207 (1998).
15. J. Simon and J.J. Andre, *Molecular Semiconductors* (Springer-Verlag, Berlin, 1985) p. 116.
16. J.P. Contour, P. Lenfant, and A.K. Vijh, J. Catal. **29**, 8 (1973).
17. S. Naka, H. Okada, H. Onnagawa, Y. Yamaguchi, and T. Tsutsui, Synth. Met. **111–112**, 331 (2000).
18. G. Horowitz, F. Kouki, P. Spearman, D. Fichou, C. Nogues, X. Pan, and F. Garnier, Adv. Mater. **8**, 242 (1996).
19. A. Brown, D.M. de Leeuw, E.J. Lous, and E.E. Havinga, Synth.Met. **66**, 257 (1994).
20. T. Suga, M. Iizuka, S. Kuniyoshi, K. Kudo, and K. Tanaka, Synth. Met. **102**, 1050 (1999).